Design and comprehensive characterization of novel fiber-optic sensor systems using fast-response luminescence-based O_2 probes

Jan Werner [a,b,*], Mathias Belz [c], Karl-Friedrich Klein [b,c], Tong Sun [a], K.T.V. Grattan [a]

[a] School of Mathematics, Computer Science and Engineering, City, University of London, Northampton Square, London EC1V 0HB, U.K
[b] THM, University of Applied Science, Wilhelm-Leuschner-Strasse 13, Friedberg 61169, Germany
[c] Lytegate GmbH, Ludwigstraße 36, Friedberg 61169, Germany

ARTICLE INFO

Keywords:
Optical fiber sensors
O_2 measurement
Oxygen sensing
Fast response time
Luminescence
Fluorescence
Microsensor
Optical sensors
Instrumentation
Fiber-optic
Commercial
Biomedical measurements

ABSTRACT

The detection of O_2 using optical techniques has now become very important and significant progress has been made in this area over the past few years. The measurement of O_2 concentration is a key parameter for diverse applications such as in life sciences, environmental monitoring, industry and biological research, and luminescence-based sensors are a valuable tool for measurements of this type. Often commercial sensors are unable to respond within a short time frame and drift over time - this demonstrates the importance of developing and validating a new technological approach. Given that need, a new sensor has been developed, with a specially-formed tip design coated with a very thin Platinum(II) 5,10,15,20-Tetrakis(2,3,4,5,6-pentafluorophenyl)-porphyrin (PtTFPP)-containing a polystyrene layer. The performance and reproducibility of the sensor design has been studied by comparing three identically fabricated sensor probes, showing that the new probe design has extreme fast response times – of a maximum value, $\Delta t_{90max} \approx 390$ ms for increasing and $\Delta t_{90max} \approx 250$ ms for decreasing O_2 concentrations. The sensors created had an accuracy of better than ± 0.03 % O_2 over the detection range investigated (between 0 % and 20 % O_2) and showed a very stable performance over many hours of use. Examining this in detail through extended continuous use, over 12 h in a 0 % O_2 solution, the probe stability was confirmed, showing a very low drift of luminescence decay time of ≈ 0.025 %/h (0.01 μs/h). Furthermore, the temperature 'cross-talk' has been studied in the important region between 25 °C and 40 °C (so that temperature corrections can be applied) and its mechanical stability, as well as allowing for compensation for any effects seen, has been confirmed. Given the success of the design developed, this work offers both an effective probe design and illustrates many important criteria for the selection of highly effective O_2-sensitive coating materials and thus their use as a measurement tool for different quality control (QC) applications in industry.

1. Introduction

The rapid and effective determination of the oxygen concentration (O_2) is very important in a large field of applications: in biomedical research, environmental monitoring, life sciences and in industry globally [1]. For example, the measurement of O_2 concentration in clinical blood analysis[2]; for quality control in the food industry [3] or even for seawater analysis [4,5] are of particular interest. McLeod *et al.* used O_2 sensors to analyze the effects of ocean warming and associated changes in food supply for larval coral reef fish as part of a recent climate change study [6]. To obtain the data relevant for eddy covariance correlation technique, small, fast sensors are required to measure the O_2 changes over sediment-water interfaces [7,8].

Conventionally, classical Clark electrodes [9] are well known and widely used for the measurement of O_2 concentration. However, these sensors can be subject to interference from stray electromagnetic fields and consume the analyte, which can be problematic for many applications [10]. As a result, fiber-optic O_2 sensors are in high demand for a variety of commercial and industrial applications. Illustrative examples of commercial products are available from PyroScience GmbH (www.pyroscience.com), Ocean Insight Inc. (www.oceaninsight.com), World Precision Instruments Inc. (www.wpiinc.com), PreSens Precision Sensing GmbH (www.presens.de), Unisense (www.unisense.com), Ohio Lumex (www.ohiolumex.com) – and many others could be mentioned.

The most popular methods for detecting O_2 concentration optically are based on absorption/reflection or luminescence measurements (intensity or decay time) using an indicator dye (often immobilized in a polymer) [11] and attached stably to a sensor tip [12]. Important device parameters, such as response time to the presence of O_2, sensitivity, the detection range and long-term stability of a sensing system, depend primarily on three main components of the sensor system: (1) the sensing element (including the choice of dye and supporting material), (2) the optical platform tailored to the optical nature of the coating, and (3) the measuring device itself (usually referred to as the instrumentation) [12,13]. Compared to a luminescence *intensity* measurement, the measurement of luminescence *decay time* alone has the advantage that it is relatively unaffected by photobleaching, stray light, or drift of electronic components, which may occur [14,15] with temperature or time, for example.

One of the most popular (and easiest to use) methods to do attach the sensitive material to the fiber tip are spin coating, dip coating or photopolymerization. Furthermore, the optical platform where the coating is attached (in this example, the fiber tip) will have a major influence on the response time, the sensitivity, the detection range, and the long-term stability of the system [16]. Fiber tip optimization can be achieved by reducing the tip size and/or the thickness of the indicator-based coating. In addition, the type of optical fiber used is important, as its physical properties significantly affect the sensor design, including the light guidance in the selected optical fiber [17,18], and these factors strongly influence the overall performance of the designed instrument.

As reported in the literature [1], a large number of synthetic indicator dyes are available today, with emission and excitation maxima in the UV to NIR range, and lifetimes of the excited-states ranging from nanoseconds to milliseconds, as well as ranging up to seconds for dyes emitting phosphorescence [10,11,13-16,19,20]. When selecting an indicator dye, criteria such as *absorption and emission spectra*, *luminescence brightness*, *luminescence decay time*, *chemical stability*, and *photostability* are critically important must be considered carefully. When monitoring O_2 in cells or in tissues, for example, the potential for interference from auto-fluorescence generated by biological substances must be taken into account. To minimize the effects of scattering and absorption of the excitation light, as well as interference with emission light in such situations, it is preferable to choose indicators with absorption bands between 590 and 650 nm and emission in the range of 730–900 nm [21,22]. In addition, when measuring very fast O_2 changes, for example in breath monitoring applications [23], sensors with very fast response times are needed – which can be achieved by employing very thin coatings and thus the need is for indicators possessing exceptional brightness. For example, Pt(II) complexes, like PtTFPP [24,25] and PtOEP [26,27], as well as Ru complexes (e.g. $[Ru(bpy)^3]^{2+}$ [28]and $[Ru(dpp)^3]^{2+}$) [29-31] represent an excellent choice for such applications.

Finally, organic polymers usually are preferred and widely used as host materials for O_2 indicator dyes [10,14,16,19,20] because of their relative stability and they are easy to source. In general, three main parameters can be used to characterize the polymers that influence the response of an optical sensor and thus of the design process in the work, in terms of sensitivity to O_2: *permeability* (P), *diffusion coefficient* (D) and *solubility* (S) [20]. Examples of commonly used materials are polystyrene [25,32,33], poly(methylmethacrylate) [34-36] and cellulose derivatives (e.g. ethyl cellulose [37]). In addition, numerous additives have been developed and applied in different ways in the sensor design – these can include: (1) *plasticizers* to tune the sensitivity; (2) *optical isolations* to reduce the interference with straylight as well as (3) *scattering particles* to improve the excitation and emission light distribution, as discussed more extensively in the literature [16,38].

Currently-reported luminescence-based sensors typically have response times to O_2 changes (Δt_{90}) over a very wide range, from 3.7 s to 100 s [39-43]. Often and in many measurement applications shorter response times are required. To achieve this, the fiber-optic O_2 sensor developed and reported in this work has been based on a new design, which has allowed the creation of a specially formed tip to give a faster response [7]. The tip design developed is based on the indicator PtTFPP (Platinum(II) 5,10,15,20-Tetrakis(2,3,4,5,6-pentafluorophenyl)-porphyrin) physically entrapped in a polymer (polystyrene), this being selected to be suitable for the physiologically important O_2 range of 0 % to 20 %. Furthermore, O_2 indicators based on Pt(II) and Pd(II) complexes *meso*-tetra(pentafluorophenyl)porphyrin (TFPP) are highly photostable and widely used – several have been evaluated as indicators for optical O_2 sensors (reported in many publications e.g. [39,43-46]) as well as have been shown to be ideal for commercial sensor designs [1]. With an absorbance maximum at 508 nm, PtTFPP can be excited with green light and shows a convenient emission spectrum in the red region (between 600 nm and 700 nm) with a large Stokes-Shift (100 – 170 nm) [39]. PtTFPP shows a relative long luminescence lifetime (~60 µs) which makes it ideal for a single luminescence lifetime sensing scheme, a scheme which is preferable for ease of detection. This dye is soluble in all organic solvents (e.g. toluene and chloroform) and it can be embedded in many polymeric matrices (e.g. polystyrene which has been selected in this work) [38].

Potential applications are in the biological and medical field where comparable coatings have already been shown to be particularly promising. For example, such a sensor based on PtTFPP immobilized in polystyrene has been successfully used for continuous analysis of O_2 concentration in subcutaneous adipose tissue by microdialysis [33]. The results have shown that the flow rate through the capillary sensor construction and the sample solution itself have a negligible influence on the sensor response. A comparable O_2-sensitve coating has been successfully used in an opto-chemical sensor systems for a continuous monitoring of blood gases in vital organs [47]. Such a sensor design (not affected by humidity), can be used to measure dissolved O_2 in seawater [48].

Looking closely on cross-sensitivities appearing in such applications, the effect of temperature changes is one of the largest sources of error in such an optical O_2 sensor, since the luminescence emission (here the measured decay time change) of Pt(II) complexes is responsive to O_2 and temperature (a ratio of the thermally activated delayed fluorescence (TADF) to phosphorescence) [49-51]. Thus, the effects of temperature on the sensor probes as well as mechanical stability were mainly investigated in this work in order to analyze any temperature and mechanical cross-sensitivities that may occur in the measurement scenarios.

2. Summary theoretical background of O_2 quenching and widely used models

The photoluminescence, which underpins the operation of the sensor probe, is a well-known process that describes the emission of photons when a molecule is excited with light that is suitably absorbed and produces emission at specific wavelengths [1,52]. In summary, the photoluminescence can be influenced by numerous processes – changes which are termed quenching – and represent a loss mechanism in the sensor scheme to be avoided. For O_2-sensitive indicator dyes the presence of molecular O_2 reduces the luminescence intensity and the lifetime due to dynamic collision quenching of O_2 molecules in the excited electronic state S_1 (see Fig. 1); and when returning back to ground state (S_0) no emission of a photon occurs. The process does not alter the molecules and is fully reversible [16,52].

The Stern-Volmer equation is a well-known approach to describe this photophysical effect caused by collision quenching of O_2:

$$\frac{I_0}{I} = \frac{\tau_0}{\tau} = 1 + K_{SV}\,[O_2] \qquad (1)$$

where τ_0 is the decay time and I_0 the luminescence intensity in absence of O_2. τ is the decay time and I the luminescence intensity in presence of O_2. K_{SV} is the Stern Volmer constant and $[O_2]$ the concentration of O_2.

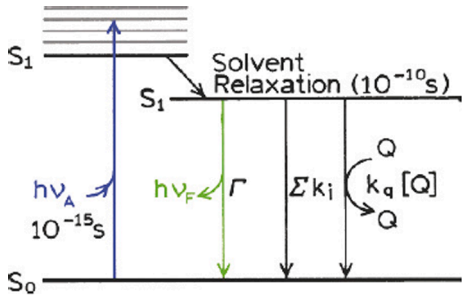

Fig. 1. Modified Jablonski Diagram illustrating the process of collision quenching [52].

However, recognizing that the Stern-Volmer equation only describes an ideal quenching system, many luminescent indicator dyes show non-linear behaviors. Thus two other popular models, Lehrer and Demas, are ideal to describe the effect of a quenchable and a non-quenchable site [1]:

$$\text{Lehrer}: \frac{I_0}{I} = \frac{\tau_0}{\tau} = \left(\frac{f}{1 + K_{SV}[O_2]} + (1 - f)\right)^{-1} \quad (2)$$

$$\text{Demas}: \frac{I_0}{I} = \frac{\tau_0}{\tau} = \left(\frac{f}{1 + K^1_{SV}[O_2]} + \frac{(1 - f)}{1 + K^2_{SV}[O_2]}\right)^{-1} \quad (3)$$

where f and (1 − f) represent the relative contribution of each site to the total luminescence emission, K^1_{SV} and K^2_{SV} are the Stern–Volmer constants for the two sites while in the Lehrer model, the constant K^2_{SV} of the second site is assumed to be zero. A wider discussion of the theoretical background to this work can be seen in the literature [1].

3. Material and methods to optimize sensor design

3.1. Preparation and fabrication of the fiber-optic O_2 sensor probes

The chemicals used to prepare the O_2 sensitive coating were PtTFPP (Frontier Scientific, Inc), PS (average M_w 2.500, Merck KGaA), chloroform (Merck KGaA) as well as toluene (Merck KGaA) and these were of analytical grade and thus, no further purification was needed. Further, three (nominally) identical probes, designated *Probe A1*, *Probe A2* and *Probe A3*, have been fabricated to allow cross-comparison, as described below.

A commercially available silica fiber 400/430 μm (core/cladding) was purchased from Polymicro Technologies and been used as the basis of the sensor probes. However, to create the high speed sensor design planned, the tip of each fiber was thermally treated to decrease the diameter of the fiber tip (<50 μm). In comparison to a 'standard' cleaved optical fiber end-face (a flat tip design), use of the taper-form increases the power fraction of the evanescent wave in the cladding of the optical fiber and thus the sensitivity to optical changes of the O_2-sensitive layer attached [53]. Following that, the tips thus prepared were chemically treated with the goal to remove remaining parts of the cladding – in that way to further increase the effective area (and thus the sensitivity of the fiber tip) over which the coating could be applied, and as well to optimize the light emission.

As a next step, the O_2-sensitve coating has been prepared by adding 140 μL PtTFPP/toluene solution (0.029 mol/L) to a 100 μL polystyrene/ solution (9.62 mol/L), using a procedure comparable to that described in the literature [25].

To form the required thin PtTFPP-containing PS layers on the fiber-optic tips, a simple and fast dip-coating process was needed. Each prepared fiber tip was first dipped into the O_2-sensitive coating composition and then quickly removed (see Fig. 2 A&B) achieving the thin and reproducible coating required.

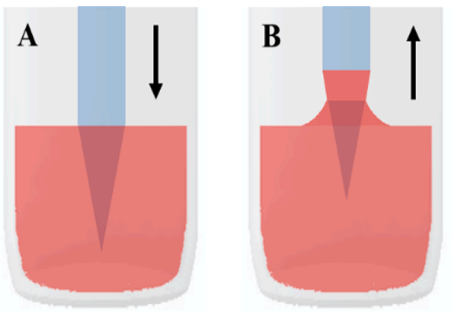

Fig. 2. Schematic illustration of the dip-coating process exemplified for a tapered sensor tip. **A**: Fiber tip moved into coating mixture (red); **B**: Adhesion of coating material (red) when fiber tip moved out of the solution.

The amount of the coating material that was left on the fiber tip (effectively the coating thickness) was found mainly to depend on the viscosity and tip withdrawal velocity (when removing the probe tip from the solution [54]). However, first experiments were undertaken and the viscosity of the coating mixture optimized, to allow repeatable coating thicknesses to be produced, with this simple dip-coating approach (in these experiments by hand), but capable of being scaled up to be automated, as has been done in previous coated fiber-optic sensors (for humidity monitoring) [55,56]. Thus, a complex motorized and velocity-controlled setup was not needed at this stage, having simplified and speeded up the production process at this experimental stage. When coated, each of the probes created was carefully dried at room temperature and under constant humidity for 24 h, to remove any residual solvent. After that process had been completed, the PtTFPP was physically entrapped in the PS matrix and the sensors were ready for a careful and systematic evaluation of their performance. In addition, a further characterization of the thickness of the coating left on the sensor tip was obtained and analyzed using a laser scanning microscope (VK-X200, KEYENCE GmbH): repeatable layer thicknesses of<0.76 μm were measured across the entire coating area.

3.2. Instrumentation used for the characterization of the O_2 probes

The requirement here has been designed for an accurate measurement of the fluorescence decay time, the parameter which encodes the O_2 data – as stated the approach used was based on direct luminescence decay time measurements of a single indicator dye. Furthermore, the required instrument must be optimized for fiber-optic sensors coated with O_2-sensitive layers as well as offering temperature compensation, at this stage with a thermistor (but an all-fiber approach to include temperature measurement could be used) [57]. Given that a commercially available device that met the requirements of the measurement of the fluorescence decay time needed was available (neoFox from Ocean Insight Inc.), this was used to characterize the O_2 probes developed here. The neoFox device chosen uses the time-domain method as the key analytical parameter to determine the decay time (and thus the O_2 concentrations [1]). This method is well known and a widely applied technique to measure the O_2-dependent luminescence decay time changes.

In the practical configuration designed and employed, the instrument was equipped with a fiber-bundle, BIFBORO-1000–2, to guide the excitation light with a peak wavelength of $\lambda_{ex.} \approx 460$ nm (see Fig. 3) to the tip of a fiber-optic sensor and then a portion of the luminescence emission back to a detector, using the other branch of the bifurcated fiber-bundle. This optical setup has the advantage of allowing the use fiber-optic O_2 probes with different diameters (e.g. from 100 μm to 1 mm), and thus different sensor sizes, while achieving a highly efficient light coupling. The excitation light source was modulated with a 'square wave' approach and a modulation frequency of 4.85 kHz, chosen to suit the decay time of the dye. Thus the determination of O_2 was achieved by

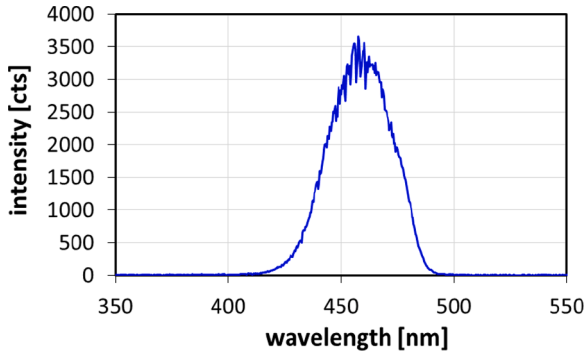

Fig. 3. Spectrum of the excitation light source of the neoFox instrument generated with a blue LED and longer wavelengths blocked with a short-pass filter.

measuring the characteristics of the decay time curve of the emission light generated from the coating on the probe.

3.3. Experimental set-up and methods used

Fig. 4 illustrates the use of the test chamber, specially designed to characterize the fiber-optic O_2 sensors, in this evaluation under constant environmental conditions. This consists of a temperature-controlled and regulated chamber, in which the O_2 concentrations used (achieving levels between 0 % and 100 % O_2) could be adjusted accurately with the use of two high accuracy and fast thermal mass flow meters/controllers (EL-FLOW Prestige, Bronkhorst LLC USA – with a maximum volume flow of 500 ml/min). These enable regulation and measurement of the gas volume flows of O_2 (purity ≥ 99,999 %) and N_2 (purity ≥ 99,999 %). In this system, the input ports of the flow meters/controllers were connected to the gas bottles used and the output ports to a gas mixer (using PTFE tubing to avoid contamination) – thus to generate well-defined O_2 concentrations. An electronically controlled valve was used to allow an automatically opening and closing of the O_2 gas mix flow into the test chamber. This valve is important to ensure a fast gas exchange inside the test chamber, especially necessary for the rapid response time analyses of the developed O_2 sensor probes which were carried out. For that set of tests, the valve used was connected close to the input port of the chamber, via a short piece of PTFE tubing. A second electronic valve was used to open and close (automatically) the gas outlet from the chamber. In combination with the first valve, this function then allowed the entire gas flow to be closed to maintain a constant O_2 concentration in the test chamber – creating a stable environment, ideal for long-term measurements under known conditions.

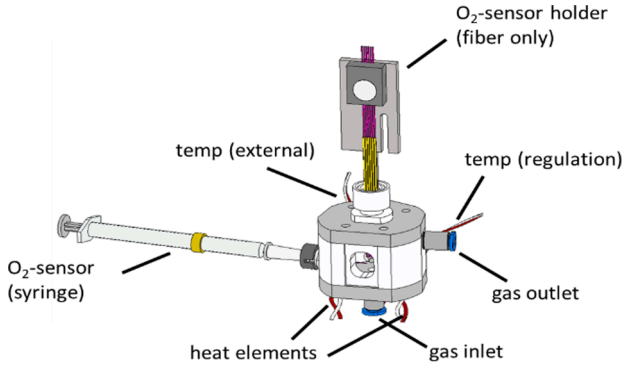

Fig. 4. Illustration of the temperature regulated (20 °C to 80 °C) test chamber to generate stable O_2 concentrations for a range of 0 % O_2 – 100 % O_2. It allows the integration of O_2 sensors in a syringe housing and sensors without housing using the O_2 sensor holder. The valves connected to the input and output ports are not shown here.

The whole body of the test chamber was constructed of aluminum components. In order to generate and regulate different temperatures (20 °C to 80 °C) inside the chamber, three heating elements were placed in the aluminum body (as well as a Pt100 used to monitor the temperature changes in this case). Furthermore, the test chamber had been designed to allow the integration of *different types of fiber-optic O_2 sensor designs* in the tests: these included O_2 sensors in a syringe housing and fiber-optic O_2 sensors (evaluating up to five simultaneously) without a housing, using an O_2 probe holder. In addition, an external temperature sensor could readily be connected for temperature compensated O_2 measurements using the neoFox device. Table 1 summarizes the specifications of the test setup specifically developed for use in this work.

To undertake a calibration and thus determine the response curves of the O_2 sensor probes, a very commonly used method [43,58,59] is to insert a sensor into a sealed chamber filled with gas of different O_2 concentrations (typically ratios of O_2 and nitrogen gas). However, this approach was not expected to be sufficiently precise, as calibrations are required for very accurate measurements of O_2. As a result, in this work a multi-point calibration, carried out under carefully controlled laboratory conditions (ensuring temperature was stabilized and well calibrated), was necessary. To undertake this, each probe that was calibrated was placed in the temperature-regulated chamber and connected to the neoFox device. Using software to control the two gas flow regulators (for O_2 and N_2) as well as the temperature, very precise O_2 concentrations from 0 % O_2 to 20 %O_2, (changed in steps of 4 % O_2), were determined for the chamber. In addition, the temperature was precisely controlled (at 25 °C), to provide repeatable calibration data not affected by temperature changes. With the gas mixture being passed through the chamber, the luminescence intensity and decay time were measured with the neoFox device, simultaneously. To obtain the data which then were fitted to the Lehrer model (see Eq. (2)), average values for the luminescence decay time were determined, over a duration of 50 s, for each O_2 concentration considered. In this case, the Lehrer model requires the estimation of 3 key parameters (τ_0, K_{SV} and f), to fit the calibration data, representing the luminescence response versus the O_2 concentration.

To undertake the calibration and determine the response time, each sensor was placed in the temperature regulated chamber ($T_{const.} = 25$ °C) and connected to the neoFox device. To do so, first, pure nitrogen (0 % O_2) was passed through the chamber for about 15 s following which the gas mix was changed to 20 % O_2. After a further 50 s, the gas mix was changed rapidly to an O_2 concentration of 0 % O_2 again. Using the data collected, the rise and fall times representing the sensor response was then determined at Δt_{90} (90 % of saturation).

To analyze the long-term drift (from the 'photo-bleaching rate') of the O_2 sensor probes, a solution containing 0 % O_2 was prepared by adding 1 g sodium sulfite (Na_2SO_3) to 10 ml distilled water and stirred for 5 min in an ultrasonic cleaner until the Na_2SO_3 was completely dissolved. This solution is ideal for long-term measurements and has a very long stability and shelf life, of approximately 96 h. In addition, measuring the signal drift at 0 % O_2 was seen as preferable, since the PtTFPP material used has its maximum luminescence emission intensity at this concentration and thus the highest overall potential bleaching rate. The set up used was as shown in Fig. 5, where after the solution was prepared, the bottle was closed with a silicone seal and the fiber-optic

Table 1
Specifications of the developed test setup used to characterize the O_2 sensors.

Parameter	Value / Range
volume flow range	0 – 1000 ml/min
response time gas regulation (at 1000 ml/min)	< 300 ms
O_2 concentration range	0 – 100 %
average O_2 accuracy	≤ 0.01 % O_2
temperature range	20 °C – 80 °C
temperature accuracy	< 0.03 °C
response time temperature regulation (25 °C to 80 °C)	< 4.5 min

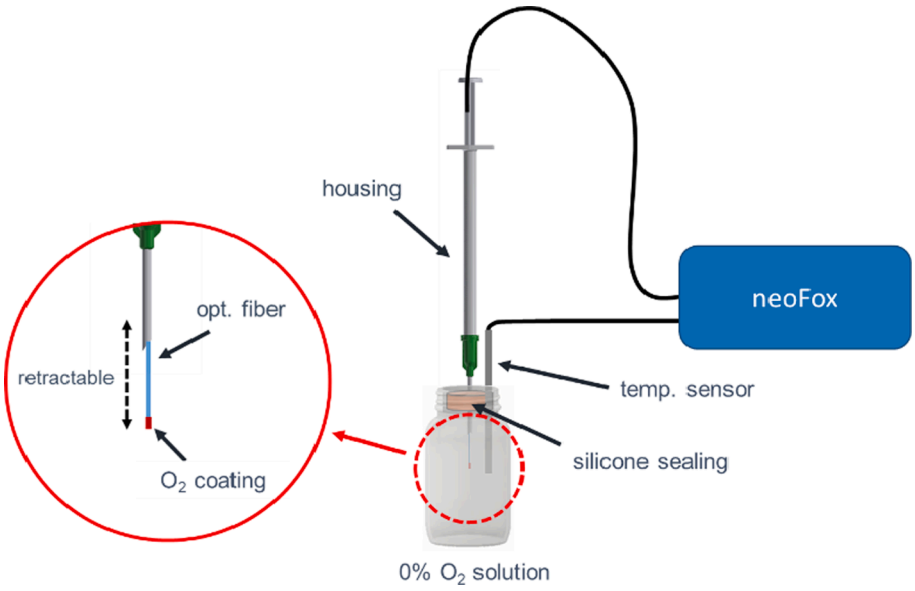

Fig. 5. Illustration of the experimental setup to evaluate the long-term stability of the fiber-optic O_2 sensors. The sensor was connected with the neoFox and maintained for 12 h in a closed bottle containing a 0 % O_2 solution. The optical fiber is protected in a retractable syringe housing.

sensor (in a syringe housing) inserted and then maintained for 12 h in the solution. To monitor the luminescence decay time and intensity as well as the temperature of the solution over time, the fiber-optic sensor and a thermistor were connected with the neoFox and the sensor tip of the O_2 probe was continuously irradiated with light pulses, (at a frequency of 4.85 kHz).

To evaluate the mechanical stability of the sensor tip and coating adhesion under strong vibrations, the tip of the fiber-optic sensors were placed in an ultrasonic cleaning bath filled with pure H_2O, in which the sensor was left for 15 min and excited with green light from the neoFox instrument. To examine whether any damage to the tip occurs (e.g. a detachment of the coating), each sensor was individually calibrated before and after the experiment was carried out.

Finally, the effect of temperature on the fiber-optic O_2 sensors was investigated (emphasizing the physiological important range between 25 °C and 40°). To do so, each sensor was placed in the temperature regulated chamber and connected to the neoFox device after which the temperature was set to 25 °C and concentrations of 0 %, 4 %, 8 %, 12 %, 16 % and 20 % O_2 were passed through the chamber for 30 s in each case. This procedure was systematically repeated when increasing the temperatures, in steps of 5 °C, until the maximum value (of 40 °C) was reached and for each temperature and O_2 concentration, the luminescence decay time (obtained from the sensor tip) was determined by averaging the signals over a time interval of 10 s.

4. Experimental results and discussion

The following sections concentrate on the results obtained from the three similarly-fabricated fiber-optic O_2 probes (designated *Probe A1, Probe A2* and *Probe A3*) using the experimental setups described above. These results are discussed and compared, emphasizing the effect of the repeatability of the manufacturing process used.

4.1. Optical and spectral properties of O_2 probes

Fig. 6 shows the typical sensor response: an O_2-dependent emission spectra of a specially tapered sensor tip when excited with light from a 470 nm LED and measured for O_2 concentrations between 0 % and 20 % O_2, in steps of 4 % O_2, using a USB2000 spectrometer (Ocean Insight Inc.). The PtTFPP-containing polystyrene coating shows a luminescence emission between 600 nm and 750 nm (with a maximum at 650 nm) and

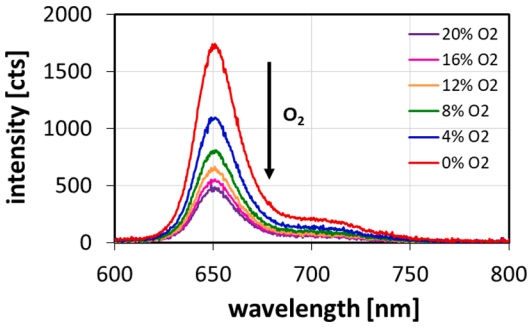

Fig. 6. O_2-dependent emission spectra of a specially tapered tip when excited with light from a 470 nm LED and measured for O_2 concentrations between 0 % and 20 % O_2 in steps of 4 % O_2.

is comparable in shape to that shown in the literature [39]. The intensity recorded changes with O_2 concentration, most significantly between 0 % and 4 % O_2, showing that the coating has the highest sensitivity for low O_2 concentrations. In addition, the special tip design (enabling the use of thinner coatings) still emits a bright luminescence emission that can easily be recorded – a positive feature of the sensor performance, allowing fast response times to be achieved without compromising the signal-to-noise ratio (SNR).

4.2. Calibration and repeatability of O_2 probes

To evaluate the repeatability of the probe with the specially tapered tip design, *Probe A1, Probe A2* and *Probe A3* were investigated, having been fabricated and coated based on the procedures described above and to cross-compare them, each probe has been calibrated individually.

Fig. 7 illustrates the luminescence decay times measured over a period of 550 s with the neoFox device, showing these for *Probe A1* (red curve), *Probe A2* (blue curve) as well as *Probe A3* (green curve) when stepping over the O_2 concentration range from 0 % to 20 % O_2. For each probe very 'clean' steps are formed as the O_2 concentration changes as the experiment progresses. The results obtained clearly show that the fiber-optic sensors based on this new tip design show a closely similar luminescence decay time response to O_2 changes, with a maximum deviation of 0.59 µs (determined at 0 % O_2) and showing that the probes

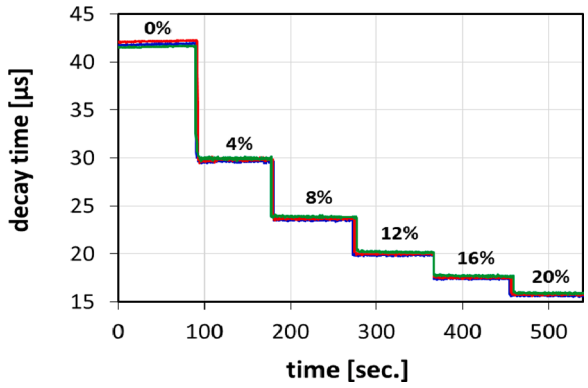

Fig. 7. Measured luminescence decay times of three fabricated O_2 probes with specially tapered tip (red: *Probe A1*; blue: *Probe A2*; green: *Probe A3*) when stepping over the range of 0 % to 20 % O_2. All results were obtained using the neoFox device.

can be manufactured with a high level of repeatability in their performance.

Furthermore, the extremely low sensor-to-sensor variation is also reflected in the calibration results shown in Fig. 8. Here, each data point has been determined in the steady state and by averaging the luminescence decay times over a time interval of 50 s (using 100 sampling points). The dashed lines represent the fitted Lehrer model by applying Eq. (2) and it can be clearly seen that this relationship describes the experimental results with a very high level of precision (max. $R^2 = 0.9999$; min. $R^2 = 0.9998$). In addition, Table 2 shows the estimated parameters (τ_0, K_{SV} and f) derived from the Lehrer model used and thus determined for the three fabricated O_2 probes. With a maximum dynamic range between 0 % and 4 % O_2, the sensors represents the highest sensitivity for low O_2 concentrations, but still a very good response for the overall measurement range shown has been achieved – all this makes this probe design very suitable for many applications, especially in the biological or medical field.

4.3. *Performance and response time of O_2 probes*

Figs. 9 to 11 give more details of the performance, showing the changes in the measured O_2 concentration for the three calibrated probes, when stepping across the range of oxygen concentrations from

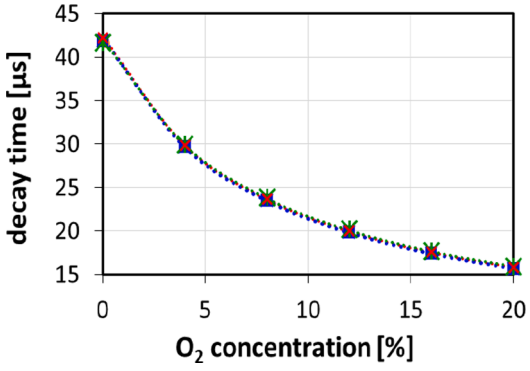

Fig. 8. Calibration curves of three fabricated O_2 probes (red: *Probe A1*; blue: *Probe A2*; green: *Probe A3*). The data points for each O_2 concentration have been determined at steady state and over the range of 50 s (100 sampling points). The dashed curves represent the fitted Lehrer model applying Eq. (2).

Table 2
Estimated parameters (τ_0, K_{SV} and f) of the fitted Lehrer model and correlation coefficient R^2 determined for the three fabricated O_2 probes.

Sensor	τ_0 [µs]	K_{SV}	f	K (=K_{SV}*f)	R^2
Probe A1	42.55	0.1313	0.8678	0.1139	0.9999
Probe A2	42.32	0.1319	0.8671	0.1144	0.9999
Probe A3	42.22	0.1273	0.8668	0.1103	0.9998

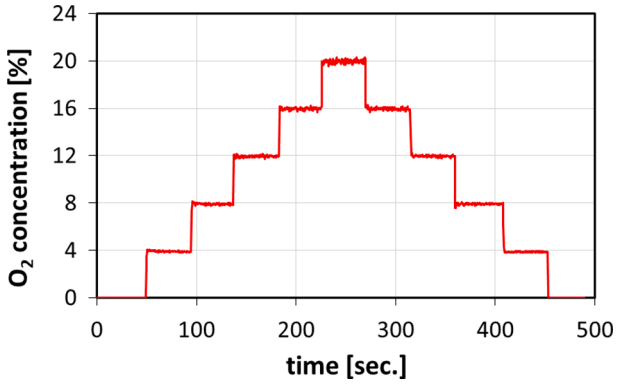

Fig. 9. Measured O_2 changes of *Probe A1* in gaseous O_2 after calibration when stepping over the range 0 % to 20 % O_2 and at a constant temperature of 25 °C.

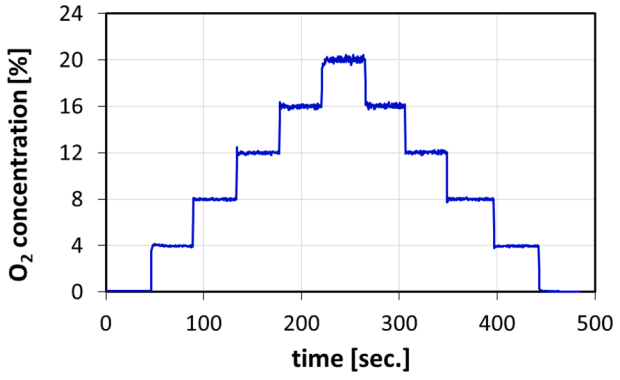

Fig. 10. Measured O_2 changes of *Probe A2* in gaseous O_2 after calibration when stepping over the range 0 % to 20 % O_2 and at a constant temperature of 25 °C.

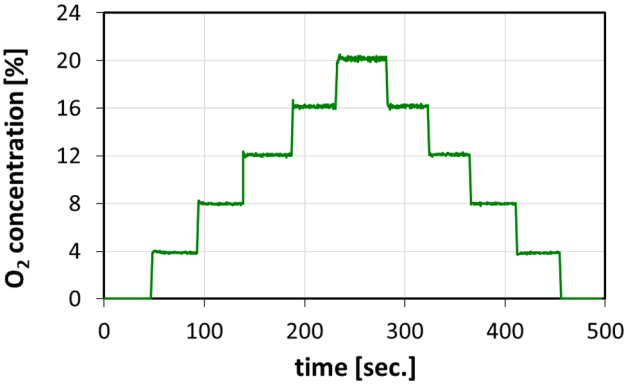

Fig. 11. Measured O_2 changes of *Probe A3* in gaseous O_2 after calibration when stepping over the range 0 % to 20 % O_2 and at a constant temperature of 25 °C.

0 % to 20 % O_2. All three sensors several of the key desired features – a highly repeatable set of measurements for increasing and decreasing O_2 concentrations, a fast response, as well with an average signal variation of ≈ 0.1 % O_2 due to the really very good signal-to-noise ratios seen. Further, the evaluation undertaken shows an average sensor accuracy in the detection of oxygen concentration of better than ± 0.03 % O_2 across the overall detection range – calibrating by using the measured volume flows of the thermal mass flow meters/controllers for N_2 and O_2 as reference (and not adding any error from this reference).

The rapid response time of the newly developed O_2 sensor design is an important feature and this has been studied in some detail and over the whole detection range from 0 % to 20 % O_2, (and back to 0 % O_2 again), using the three fabricated probes, as shown in Figs. 12 to 14. This innovative sensor design show very fast response times of $\Delta t_{90min} \approx 230$ ms and $\Delta t_{90max} \approx 390$ ms for *increasing* O_2 concentrations, and an even faster response time of $\Delta t_{90min} \approx 190$ ms and $\Delta t_{90max} \approx 250$ ms for *decreasing* O_2 concentrations – determined from the sensor set prepared. The response time is influenced positively by the narrow profile tip design, which allows very thin coatings, yet still the detection of luminescence signals over a large effective area of the tip, allowing a much faster diffusion of O_2. Further tests carried out show that the probes have a comparable, and rapid response to O_2 changes for the overall studied O_2 range. Such a very fast response time is an important features and advantage of the probe design, giving a performance that compares well to the data published on other optical sensor designs with comparable PtTFPP- or PtOEP-containing coatings, as such sensor designs typically show response times between 3.7 s and 100 s [39-43], which are longer than for the probe reported.

4.4. *Long-term stability of O_2 probes*

Fig. 15 shows the results of a series of longer-term measurements made in a stable 0 % O_2 solution, for an extended period of 12 h, subjecting the probes to continuous irradiation with light pulses ($f_{pulse} = 4.85$ kHz) at the same time, to investigate any drift of luminescence decay time (Fig. 15A) and intensity (Fig. 15B), generated by photobleaching of the indicator. Each measurement was taken in an almost temperature-stable environment (to ensure this, the temperature was monitored and has been found to be very stable ($\Delta T_{max} \approx 0{,}46$ °C) over the entire measurement time (Fig. 15C)). It was pleasing to note that the three fabricated sensors (data in Fig. 15 are shown as follows – *Probe A1*: red, *Probe A2*: blue, *Probe A3*: green) were extremely stable and have a maximum drift of luminescence decay time of $\Delta\tau_{max} \approx 0.025$ %/h (0.01 µs/h). Highlighting *Probe A3*, the drift with $\Delta\tau_{max,A3} \approx 0.007$ %/h was the lowest and showed the highest stability of all three sensors. Furthermore, the results clearly show that a measurement of luminescence decay time is significantly less affected by either photobleaching or instability (drift) of the light sources, as well as the sensitivity of the photodetectors – this time domain approach comparing favorably with a scheme using a measurement of luminescence intensity ($\Delta I_{max} \approx 1$ %/h). However, even for this extreme situation of continuous irradiation with light pulses and a sampling rate of 0.5 s, the sensors show an exceptional long-term stability with the advantage to reduce the frequency of re-calibration of the probe. For many applications where a measurement error of ≈ 0.5 % O_2 (for O_2 concentrations < 20 % O_2) is allowed, a sensor would then need a re-calibration after 144,000 data points or 20 h of a continuous measurement with a sampling rate of 0.5 s – which is much longer than is needed for many biomedical applications. A further important feature of the probe design is the higher sensitivity of the sensor at very low O_2 concentrations (<4 %O_2). Thus here a re-calibration after a longer period of 890,000 data points (or a measurement duration of 124 h) would be needed for measurements in this O_2 region.

4.5. *Mechanical stability of O_2 probes*

Fig. 16 shows the average calibration values obtained from the three probes before and after exposure to vibration. Here the sensors were left for 15 min in a commercial ultrasonic cleaner filled with H_2O, to investigate whether any mechanical damage to the tip during exposure or a signal change due to detachment of the O_2-sensitive coating occurs. Excellent performance is seen in that the PtTFPP-containing PS coating shows a strong adhesion to the fiber tip surface and no mechanical damage could be observed when the tip was examined under a microscope. Fig. 17 shows the images of *Probe A1* before and after the sensor was held in an ultrasonic cleaner. Comparing the calibration curves

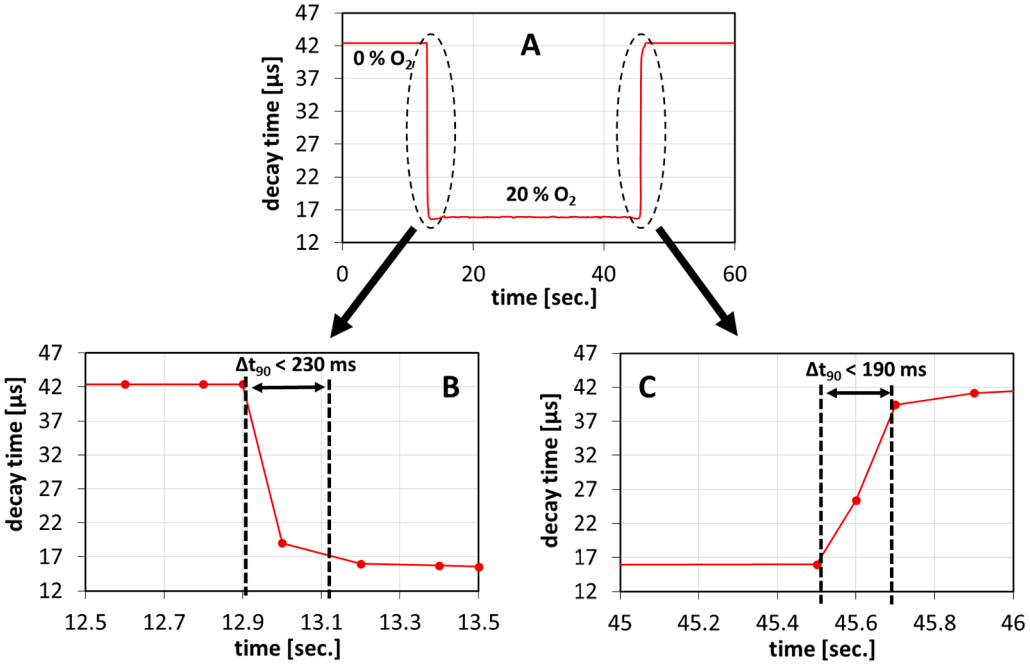

Fig. 12. Measured response time of *Probe A1* due to a rapid change from 0 % to 20 % O_2 and back to 0 % O_2 again (**A**). (**B**) shows the rise time (*increasing O_2 concentrations*) of the probe ($\Delta t_{90} \approx 230$ ms) and (**C**) the fall time (*decreasing O_2 concentrations*) of the probe ($\Delta t_{90} \approx 190$ ms).

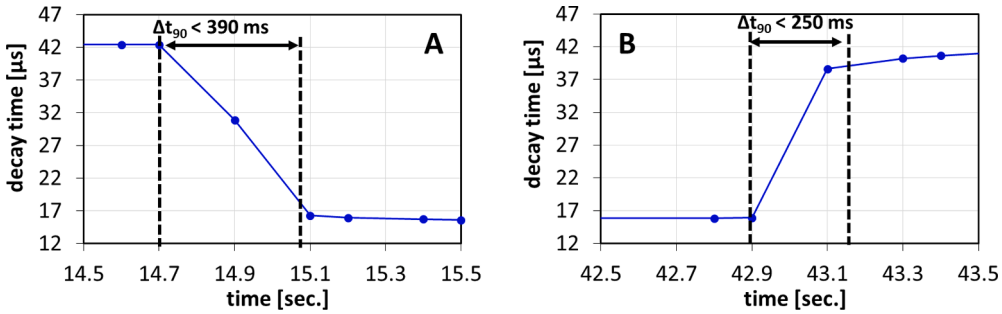

Fig. 13. Measured response time of *Probe A2* due to a rapid change from 0 % to 20 % O_2 and back to 0 % O_2 again. (**A**) shows the rise time (*increasing O_2 concentrations*) of the probe ($\Delta t_{90} \approx 390$ ms) and (**B**) the fall time (*decreasing O_2 concentrations*) of the probe ($\Delta t_{90} \approx 250$ ms).

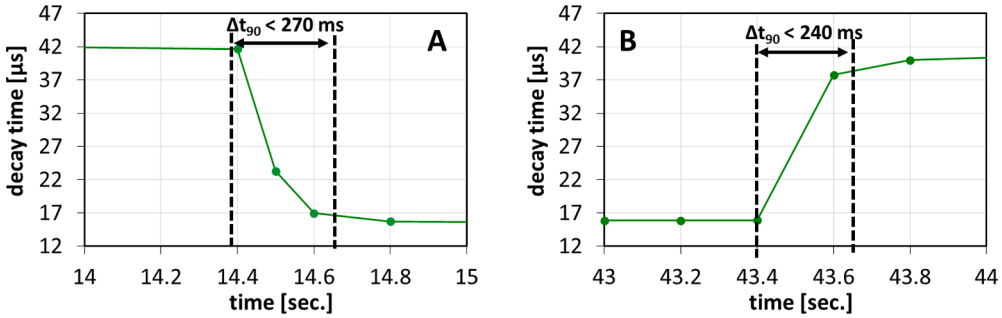

Fig. 14. Measured response time of *Probe A3* due to a rapid change from 0 % to 20 % O_2 and back to 0 % O_2 again. (**A**) shows the rise time (*increasing O_2 concentrations*) of the probe ($\Delta t_{90} \approx 270$ ms) and (**B**) the fall time (*decreasing O_2 concentrations*) of the ($\Delta t_{90} \approx 240$ ms).

during these tests, no significant signal changes have been measured and this indicates that no detachment of the coating occurred during the experiment. Importantly, the results show that the sensor could be used in harsh environments where it is mechanically stressed without the need of a re-calibration. Furthermore, the probe is not influenced to any other physical effects that occur during the ultrasonic irradiation (used here to create the vibration).

4.6. *Effect of temperature on O_2 probes*

Since the change in calibration due to any temperature drift is likely to be the biggest source of error in optical luminescence-based sensors, the effect of temperature has been studied over temperature range between 25 °C and 40 °C and in steps of 5 °C using the setup and procedure described above. Fig. 18 exemplary shows the calibration curve obtained of *Probe A1* illustrating the temperature 'cross-talk'. Repeating the experiment, *Probe A2* and *Probe A3* showed a comparable behavior to temperature changes.

The results show the expected effect on the luminescence lifetime, as it shortens the luminescence lifetimes of PtTFPP for increasing temperature values (and indeed this approach has been used very effectively in stand-alone temperature sensors [60]). The calibration curves obtained show an overall shift to lower decay times for increasing temperatures.

Investigating the relationship between the luminescence decay time and the temperature changes in more detail, Fig. 19 shows the normalized luminescence decay times with temperature for the three fabricated probes, over the O_2 range used. The temperature-induced signal drift shows a linear behavior over the O_2 range shown (between 0 % and 20 % O_2). Comparing the performance of all three probes, for O_2 concentrations ≥ 8 % O_2 the sensor design shows an almost similar relative signal drift of $\Delta\tau_{min,8\%} \approx 0.41$ %/°C (*Probe A1*) and $\Delta\tau_{max,8\%} \approx 0.56$ %/°C (*Probe A3*). For O_2 concentrations of < 4 % O_2, the relative drift of luminescence decay time is slightly lower and measured to be $\Delta\tau_{min,0\%} \approx 0.10$ %/°C (*Probe A1*) and $\Delta\tau_{max,0\%} \approx 0.21$ %/°C (*Probe A3*) determined at 0 % O_2, as well as $\Delta\tau_{min,4\%} \approx 0.30$ %/°C (*Probe A1*) and $\Delta\tau_{max,4\%} \approx 0.41$ %/°C (*Probe A3*) at 4 %O_2. However, this effect is due to the nonlinear response of the coating material to O_2 changes, so that temperature changes at higher O_2 concentrations have a greater effect on the measured luminescence decay time.

The results obtained show a high temperature stability of the sensor probes themselves. Looking closely, while *Probe A1* shows the lowest 'cross-talk' to temperature changes, *Probe A3* illustrates the maximum decrease in luminescence decay time for increasing temperature values, over the O_2 range analyzed. However, the results assume that small variations seen during sensor fabrication, such as the amount of O_2-sensitive material attached to the fiber tip or inhomogeneity in the layer thickness also affect the sensor response to temperature. These changes are not significant, but must be taken into account when larger number of O_2 probes are to be fabricated (for example in commercial exploitation), to achieve the highest level of accuracy in the probe. It is easy to include temperature compensation by incorporating a further temperature sensing element in the probe (e.g. a small length of rare-earth doped fiber whose decay time will also change with temperature, but is unaffected by O_2 concentration changes [61], or to include a Fiber Bragg Grating or a Long Period Grating temperature sensor [62]).

5. Conclusions

The paper has focused on reporting the comprehensive results of a design and performance optimization, including key fabrication issues, of a new fast fiber optic based probe design. Several new designs of fiber optic-based O_2 sensor probes have been developed and evaluated. In so doing, three identical sensors (*Probe A1 to A3*) were fabricated and their performance characteristics examined in light of the literature and key performance criteria and the results cross-compared. The results of this extensive study of key parameters are very promising and show that the new probe design significantly improves the sensor performance when compared to conventional sensor designs. The key feature of the probe design is that the sensors show an extremely fast response time of

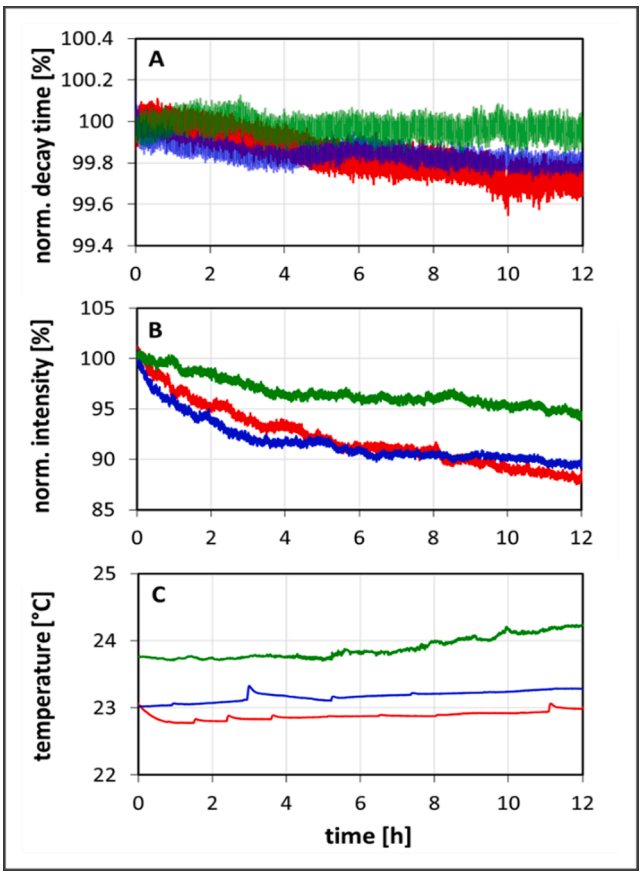

Fig. 15. Decrease of luminescence decay times (**A**) and intensities (**B**) seen under continuous irradiation for 12 h of *Probe A1* (red), *Probe A2* (blue) and *Probe A3* (green) placed in in a stable 0 % O_2 solution. Each measurement performed in an almost temperature-stable environment (**C**).

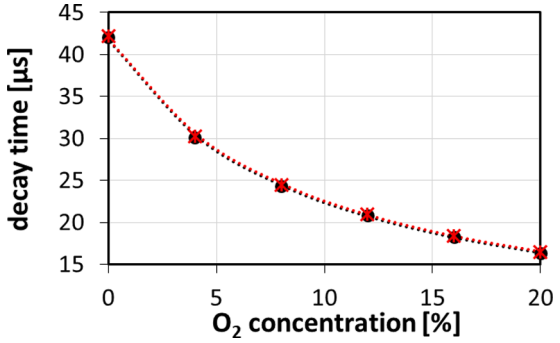

Fig. 16. Average calibration values of the three probes in gaseous O_2 before (black) and after (red) the sensors were hold in an ultrasonic cleaner for 15 min. The dashed curves represent the fitted Lehrer model applying Eq. (2).

$\Delta t_{90max} \approx 390$ ms (increasing O_2) and $\Delta t_{90min} \approx 190$ ms (decreasing O_2). The performance achieved was found to depend on the unique characteristics seen, resulting from the increased effective area of what was still a very compact sensor tip, allowing an optimization of the light emission from the probe and permitting the use of thinner coatings on the fiber tip itself without compromising the signal-to-noise ratio. Given the sensor performance reported, highly accurate measurements (to better than $\pm$ 0.03 % O_2 in the range of 0 % O_2 to 20 % O_2) were shown to be possible. Because of the design characteristic that used small optical fibers and small fiber tip diameters, the sensors are well suited to the measurement of very small gas volumes – making them potentially very

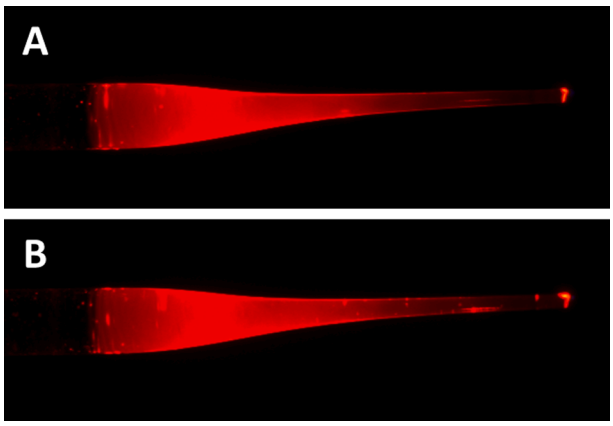

Fig. 17. Images of *Probe A1* (**A**) before and (**B**) after the sensor was held in an ultrasonic cleaner for 15 min, showing the red emission light of the PtTFPP-containing polystyrene coating when excited with light from a UV LED.

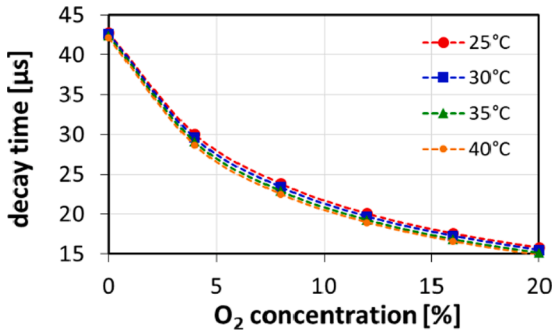

Fig. 18. Influence of temperature on the calibration curve of *Probe A1* for a temperature range between 25 °C and 40 °C. Each data point has been determined by averaging the measured signals over a time frame of 10 s at steady state.

attractive in biomedical applications. A further positive feature of these sensors is that they are usable with commercially available (decay time monitoring) devices and thus in combination with the commercial signal processing unit used, have been shown to be very stable in studies carried out over a long period of time. For example, during measurements for 12 h in a stable 0 % O_2 solution and with continuous irradiation of light (pulsed at f = 4.85 kHz), a very low signal drift of the decay time and a negligible influence of stray light (from the source) were observed. However, even for this extreme situation the sensors show an exceptional long-term stability – thereby reducing the need for re-calibration. Due to the very low sensor-to-sensor variation and the exceptional long-term stability, a potential user only would need to re-calibrate the sensors after a long period of time – ideal for commercial uses of such sensors.

Furthermore, the important temperature 'cross-talk' that can be a problem in many such sensor designs was investigated in the physiologically relevant temperature range between 25 °C and 40 °C. The results obtained show a really good temperature stability of the sensor design itself and, most importantly, a linear relationship between temperature and decay time. When highly accurate measurements of O_2 concentration between 25 °C and 40 °C are required, this allows a relative simple temperature compensation by incorporating a further fiber optic based temperature sensor in the probe, building on previous work by some of the authors.

A very positive conclusion of this study is that it has been clearly demonstrated that the new probe design has the potential to expand the range of applications for fiber optic O_2 sensors by taking full advantage of the fast response times of this design. A further benefit of this design is

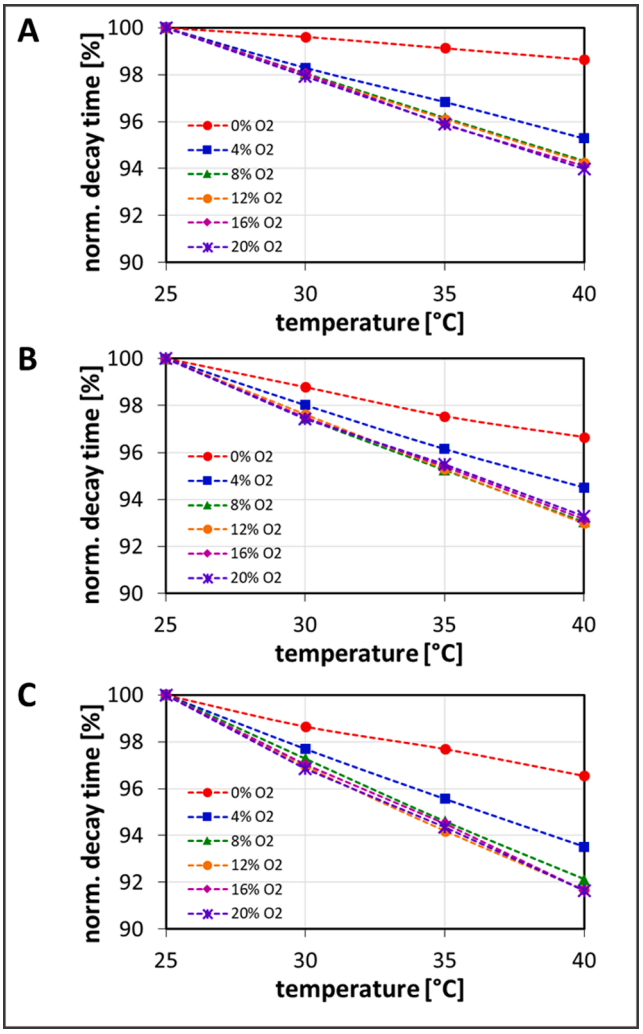

Fig. 19. Effect of temperature on the sensor design (**A**: *Probe A1*; **B**: *Probe A2* and **C**: *Probe A3*) showing the normalized luminescence decay times over temperature (between 25 °C and 40 °C) determined for O_2 concentrations between 0 % and 20 % O_2.

that sensors can be manufactured with a high level of repeatability using a simple and fast dip-coating process and thus 'scale-up' to volume production, at low cost, is feasible. The range of characterization experiments carried out provide the basis of a quality control (QC) regime for a manufacturer.

CRediT authorship contribution statement

Jan Werner: Methodology, Software, Investigation, Validation, Visualization, Writing – original draft. **Mathias Belz:** Writing – review & editing. **Karl-Friedrich Klein:** Writing – review & editing. **Tong Sun:** Writing – review & editing. **K.T.V. Grattan:** Writing – review & editing.

Declaration of Competing Interest

The authors declare that they have no known competing financial interests or personal relationships that could have appeared to influence the work reported in this paper.

Acknowledgements

The authors wish to acknowledge Alexander Feger for his major support in the development and evaluation of the O_2 test chamber and would like to thank WPI GmbH for the financial support. Kenneth Grattan and Tong Sun acknowledge support from the Royal Academy of Engineering.

References

[1] J. Werner, M. Belz, K.-F. Klein, T. Sun, K.T.V. Grattan, Fiber optic sensor designs and luminescence-based methods for the detection of oxygen and pH measurement, Measurement 178 (2021) 109323, https://doi.org/10.1016/j.measurement.2021.109323.
[2] S. Kojima, H. Suzuki, A Micro Sensing System for Blood Gas Analysis Constructed With Stacked Modules, IEEJ Trans. SM 124 (4) (2004) 111–116, https://doi.org/10.1541/ieejsmas.124.111.
[3] D.B. Papkovsky, N. Papkovskaia, A. Smyth, J. Kerry, V.I. Ogurtsov, Phosphorescent sensor approach for non-destructive measurement of oxygen in packaged foods: optimisation of disposable oxygen sensors and their characterization over a wide temperature range, Anal. Lett. 33 (9) (2000) 1755–1777, https://doi.org/10.1080/00032710008543157.
[4] J.F. Gouin, F. Baros, D. Birot, J.C. André, A fibre-optic oxygen sensor for oceanography, Sens. Actuators B: Chem. 39 (1–3) (1997) 401–406, https://doi.org/10.1016/S0925-4005(97)80242-0.
[5] C.R. Schröder, B.M. Weidgans, I. Klimant, pH fluorosensors for use in marine systems, The Analyst 130 (6) (2005) 907–916, https://doi.org/10.1039/B501306B.
[6] I. M. McLeod *et al.,* "Climate change and the performance of larval coral reef fishes: the interaction between temperature and food availability," *Conservation physiology*, vol. 1, no. 1, cot024, 2013, doi: 10.1093/conphys/cot024.
[7] L. Chipman, M. Huettel, P. Berg, V. Meyer, I. Klimant, R. Glud, F. Wenzhoefer, Oxygen optodes as fast sensors for eddy correlation measurements in aquatic systems, Limnol. Oceanogr. Methods 10 (5) (2012) 304–316, https://doi.org/10.4319/lom.2012.10.304.
[8] P. Berg, M. Huettel, Monitoring the seafloor using the noninvasive eddy correlation technique: integrated benthic exchange dynamics, Oceanog. 21 (4) (2008) 164–167.
[9] L.C. Clark, R. Wolf, D. Granger, Z. Taylor, Continuous recording of blood oxygen tensions by polarography, J. Appl. Physiol. 6 (3) (1953) 189–193, https://doi.org/10.1152/jappl.1953.6.3.189.
[10] X.-D. Wang, O.S. Wolfbeis, Fiber-optic chemical sensors and biosensors (2008–2012), Anal. Chem. 85 (2) (2013) 487–508, https://doi.org/10.1021/ac303159b.
[11] M. Quaranta, S.M. Borisov, I. Klimant, Indicators for optical oxygen sensors, Bioanal. Rev. 4 (2–4) (2012) 115–157, https://doi.org/10.1007/s12566-012-0032-y.
[12] D. Wencel, T. Abel, C. McDonagh, Optical chemical pH sensors, Anal. Chem. 86 (1) (2014) 15–29, https://doi.org/10.1021/ac4035168.
[13] C. McDonagh, C.S. Burke, B.D. MacCraith, Optical chemical sensors, Chem. Rev. 108 (2) (2008) 400–422, https://doi.org/10.1021/cr068102g.
[14] X.-D. Wang, O.S. Wolfbeis, Fiber-optic chemical sensors and biosensors (2013–2015), Anal. Chem. 88 (1) (2016) 203–227.
[15] X.-D. Wang, O.S. Wolfbeis, Fiber-optic chemical sensors and biosensors (2015–2019), Anal. Chem. 92 (1) (2020) 397–430.
[16] X.-D. Wang, O.S. Wolfbeis, Optical methods for sensing and imaging oxygen: materials, spectroscopies and applications, Chem. Soc. Rev. 43 (10) (2014) 3666–3761, https://doi.org/10.1039/C4CS00039K.
[17] Arne Wilhelm Zimmer, Philipp Raithel, Mathias Belz, Karl-Friedrich Klein, "Analysis of spectral light guidance in specialty fibers," *in Proc. SPIE 9886-34*, 2016.
[18] K.-F. Klein, C.P. Gonschior, X.Ruan, M.Bloos, G.Hillrichs, H.Poisel, "Transmission of skew modes in polymer- and silica-based step-index fibers," *Proc. 18th POF-conference*, no. 45, 2009.
[19] O. S. Wolfbeis, "Luminescent sensing and imaging of oxygen: fierce competition to the Clark electrode," *BioEssays : news and reviews in molecular, cellular and developmental biology*, vol. 37, no. 8, pp. 921–928, 2015, doi: 10.1002/bies.201500002.
[20] Y. Amao, Probes and polymers for optical sensing of oxygen, Microchimica Acta 143 (1) (2003) 1–12, https://doi.org/10.1007/s00604-003-0037-x.
[21] I. Dunphy, S.A. Vinogradov, D.F. Wilson, Oxyphor R2 and G2: phosphors for measuring oxygen by oxygen-dependent quenching of phosphorescence, Anal. Biochem. 310 (2) (2002) 191–198, https://doi.org/10.1016/s0003-2697(02)00384-6.
[22] A. Vogel, V. Venugopalan, Mechanisms of pulsed laser ablation of biological tissues, Chem. Rev. 103 (2) (2003) 577–644, https://doi.org/10.1021/cr010379n.
[23] C.S. Burke, J.P. Moore, D. Wencel, A.K. McEvoy, B.D. MacCraith, Breath-by-breath measurement of oxygen using a compact optical sensor, J. Biomed. Opt. 13 (1) (2008) 14027, https://doi.org/10.1117/1.2870092.
[24] S.-W. Lai, Y.-J. Hou, C.-M. Che, H.-L. Pang, K.-Y. Wong, C.K. Chang, N. Zhu, Electronic spectroscopy, photophysical properties, and emission quenching studies of an oxidatively robust perfluorinated platinum porphyrin, Inorg. Chem. 43 (12) (2004) 3724–3732, https://doi.org/10.1021/ic049902h.
[25] S.-K. Lee, I. Okura, Photostable optical oxygen sensing material: platinum tetrakis (pentafluorophenyl)porphyrin Immobilized in Polystyrene, Anal. Commun. 34 (6) (1997) 185–188, https://doi.org/10.1039/A701130J.
[26] D.B. Papkovsky, G.V. Ponomarev, W. Trettnak, P. O'Leary, Phosphorescent complexes of porphyrin ketones: optical properties and application to oxygen

sensing, Anal. Chem. 67 (22) (1995) 4112–4117, https://doi.org/10.1021/ac00118a013.
[27] Y. Amao, I. Okura, Optical oxygen sensing properties of Tris (4,7′-diphenyl-1,10′-phenanthroline) ruthenium (II)-polyacrylic acid complex thin film, Polym J 32 (5) (2000) 452–455, https://doi.org/10.1295/polymj.32.452.
[28] M.J. Cook, et al., Luminescent metal complexes. Part 1. Tris-chelates of substituted 2,2′-bipyridyls with ruthenium (II) as dyes for luminescent solar collectors, J. Chem. Soc., Perkin Trans. 2 (8) (1984) 1293–1301, https://doi.org/10.1039/P29840001293.
[29] E.R. Carraway, J.N. Demas, B.A. DeGraff, J.R. Bacon, Photophysics and photochemistry of oxygen sensors based on luminescent transition-metal complexes, Anal. Chem. 63 (4) (1991) 337–342, https://doi.org/10.1021/ac00004a007.
[30] J.R. Bacon, J.N. Demas, Determination of oxygen concentrations by luminescence quenching of a polymer-immobilized transition-metal complex, Anal. Chem. 59 (23) (2002) 2780–2785, https://doi.org/10.1021/ac00150a012.
[31] P.C. Alford, M.J. Cook, A.P. Lewis, G.S.G. McAuliffe, V. Skarda, A.J. Thomson, J. L. Glasper, D.J. Robbins, Luminescent metal complexes. Part 5. Luminescence properties of ring-substituted 1,10-phenanthroline tris-complexes of ruthenium(II), J. Chem. Soc., Perkin Trans. (5) (1985) 705, https://doi.org/10.1039/p29850000705.
[32] E. Schmälzlin, J.T. van Dongen, I. Klimant, B. Marmodée, M. Steup, J. Fisahn, P. Geigenberger, H.-G. Löhmannsröben, An optical multifrequency phase-modulation method using microbeads for measuring intracellular oxygen concentrations in plants, Biophys. J. 89 (2) (2005) 1339–1345, https://doi.org/10.1529/biophysj.105.063453.
[33] A. Bizzarri, H. Koehler, M. Cajlakovic, A. Pasic, L. Schaupp, I. Klimant, V. Ribitsch, Continuous oxygen monitoring in subcutaneous adipose tissue using microdialysis, Analytica Chimica Acta 573-574 (2006) 48–56, https://doi.org/10.1016/j.aca.2006.03.101.
[34] A. Mills, M. Thomas, Fluorescence-based thin plastic film ion-pair sensors for oxygen, Analyst 122 (1) (1997) 63–68, https://doi.org/10.1039/A606124I.
[35] P.M. Gewehr, D.T. Delpy, Optical oxygen sensor based on phosphorescence lifetime quenching and employing a polymer immobilised metalloporphyrin probe. Part 2. sensor membranes and results, Med. Biol. Eng. Comput. 31 (1) (1993) 11–21, https://doi.org/10.1007/BF02446880.
[36] A. Mills, A. Lepre, Controlling the response characteristics of luminescent porphyrin plastic film sensors for oxygen, Anal. Chem. 69 (22) (1997) 4653–4659, https://doi.org/10.1021/ac970430g.
[37] G. Liebsch, I. Klimant, B. Frank, G. Holst, O.S. Wolfbeis, Luminescence lifetime imaging of oxygen, pH, and carbon dioxide distribution using optical sensors, Appl. Spectrosc. 54 (4) (2000) 548–559, https://doi.org/10.1366/0003702001949726.
[38] A. Apostolidis, Combinatorial approach for development of optical gas sensors - concept and application of high-throughput experimentation, Universität Regensburg (2005).
[39] C.-S. Chu, Y.-L. Lo, High-performance fiber-optic oxygen sensors based on fluorinated xerogels doped with Pt(II) complexes, Sens. Actuators B: Chem. 124 (2) (2007) 376–382, https://doi.org/10.1016/j.snb.2006.12.049.
[40] G. Holst, R.N. Glud, M. Kühl, I. Klimant, A microoptode array for fine-scale measurement of oxygen distribution, Sens. Actuators B: Chem. 38 (1–3) (1997) 122–129, https://doi.org/10.1016/S0925-4005(97)80181-5.
[41] S.-K. Lee, I. Okura, Optical sensor for oxygen using a porphyrin-doped sol-gel glass, Analyst 122 (1) (1997) 81–84, https://doi.org/10.1039/A604885D.
[42] S.-K. Lee, I. Okura, Photoluminescent determination of oxygen using metalloporphyrin-polymer sensing systems, Spectrochim. Acta Part A: Mol. Biomol. Spectrosc. 54 (1) (1998) 91–100, https://doi.org/10.1016/S1386-1425(97)00206-0.
[43] G.R. McDowell, A.S. Holmes-Smith, M. Uttamlal, C. Mitchell, P.H. Shannon, "A robust and reliable optical trace oxygen sensor", *SPIE*, Opt. Sens. 10231 (2017), https://doi.org/10.1117/12.2265561.
[44] C.-S. Chu, C.-A. Lin, Optical fiber sensor for dual sensing of temperature and oxygen based on PtTFPP/CF embedded in sol–gel matrix, Sens. Actuators B: Chem. 195 (2014) 259–265, https://doi.org/10.1016/j.snb.2014.01.032.
[45] C.-S. Chu, T.-H. Lin, A new portable optical sensor for dual sensing of temperature and oxygen, Sens. Actuators B: Chem. 202 (2014) 508–515, https://doi.org/10.1016/j.snb.2014.05.125.
[46] C.-S. Chu, Y.-L. Lo, Highly sensitive and linear calibration optical fiber oxygen sensor based on Pt(II) complex embedded in sol–gel matrix, Sens. Actuators B: Chem. 155 (1) (2011) 53–57, https://doi.org/10.1016/j.snb.2010.11.023.
[47] M. ajlakovi, A. Bizzarri, G. H., I. Knez, M. Suppan, I. Ovina, V. Ribitsch, in: Advances in Chemical Sensors, InTech, 2012, https://doi.org/10.5772/32177.
[48] C. Staudinger, M. Strobl, J.P. Fischer, R. Thar, T. Mayr, D. Aigner, B.J. Müller, B. Müller, P. Lehner, G. Mistlberger, E. Fritzsche, J. Ehgartner, P.W. Zach, J. S. Clarke, F. Geißler, A. Mutzberg, J.D. Müller, E.P. Achterberg, S.M. Borisov, I. Klimant, A versatile optode system for oxygen, carbon dioxide, and pH measurements in seawater with integrated battery and logger, Limnol. Oceanogr. Methods 16 (7) (2018) 459–473, https://doi.org/10.1002/lom3.10260.
[49] M. Schäferling, The art of fluorescence imaging with chemical sensors, Angew. Chem. Int. Ed. 51 (15) (2012) 3532–3554.
[50] P.W. Zach, S.A. Freunberger, I. Klimant, S.M. Borisov, Electron-deficient near-infrared Pt(II) and Pd(II) benzoporphyrins with dual phosphorescence and unusually efficient thermally activated delayed fluorescence: first demonstration of simultaneous oxygen and temperature sensing with a single emitter, ACS Appl. Mater. Interfaces 9 (43) (2017) 38008–38023, https://doi.org/10.1021/acsami.7b10669.
[51] S.E. Zieger, A. Steinegger, I. Klimant, S.M. Borisov, TADF-emitting Zn(II)-benzoporphyrin: an indicator for simultaneous sensing of oxygen and temperature, ACS sensors 5 (4) (2020) 1020–1027, https://doi.org/10.1021/acssensors.9b02512.
[52] J.R. Lakowicz (Ed.), Principles of Fluorescence Spectroscopy, Springer US, Boston, MA, 2006.
[53] S. Guo, S. Albin, Transmission property and evanescent wave absorption of cladded multimode fiber tapers, Optics Express 11 (3) (2003) 215–223, https://doi.org/10.1364/OE.11.000215.
[54] D. Quéré, FLUID COATING ON A FIBER, Annu. Rev. Fluid Mech. 31 (1) (1999) 347–384, https://doi.org/10.1146/annurev.fluid.31.1.347.
[55] L. Alwis, K. Bremer, T. Sun, K.T.V. Grattan, Analysis of the characteristics of PVA-coated LPG-based sensors to coating thickness and changes in the external refractive index, IEEE Sensors J. 13 (3) (2013) 1117–1124, https://doi.org/10.1109/JSEN.2012.2230534.
[56] B. Rente, M. Fabian, M. Vidakovic, L. Vorreiter, H. Bustamante, T. Sun, K.T. V. Grattan, Extended study of fiber optic-based humidity sensing system performance for sewer network condition monitoring, IEEE Sens. J. 21 (6) (2021) 7665–7671, https://doi.org/10.1109/JSEN.2021.3050341.
[57] M.R. Mokhtar, T. Sun, K.T.V. Grattan, Bragg grating packages with nonuniform dimensions for strain and temperature sensing, IEEE Sens. J. 12 (1) (2012) 139–144, https://doi.org/10.1109/JSEN.2011.2134845.
[58] Y. Xiong, J. Tan, C. Wang, Y. Zhu, S. Fang, J. wu, Q. Wang, M. Duan, A miniaturized oxygen sensor integrated on fiber surface based on evanescent-wave induced fluorescence quenching, J. Lumin. 179 (2016) 581–587, https://doi.org/10.1016/j.jlumin.2016.08.005.
[59] C.-S. Chu, C.-Y. Chuang, Highly sensitive fiber-optic oxygen sensor based on palladium tetrakis (4-carboxyphenyl)porphyrin doped in ormosil, J. Lumin. 154 (2014) 475–478, https://doi.org/10.1016/j.jlumin.2014.05.025.
[60] T. Sun, Z.Y. Zhang, K.T.V. Grattan, A.W. Palmer, Ytterbium-based fluorescence decay time fiber optic temperature sensor systems, Rev. Scientific Instru. 69 (12) (1998) 4179–4185, https://doi.org/10.1063/1.1149267.
[61] T. Sun, Z.Y. Zhang, K.T.V. Grattan, Erbium/ytterbium fluorescence based fiber optic temperature sensor system, Rev. Sci. Instrum. 71 (11) (2000) 4017, https://doi.org/10.1063/1.1289682.
[62] S.K. Abi Kaed Bey, T. Sun, K.T.V. Grattan, Sensitivity enhancement of long period gratings for temperature measurement using the long period grating pair technique, Sens. Actuators A: Phys. 141 (2) (2008) 314–320, https://doi.org/10.1016/j.sna.2007.10.019.